ORIGINAL ARTICLE

Study on tool wear characteristics in diamond turning of reaction-bonded silicon carbide

Zhiyu Zhang · Jiwang Yan · Tsunemoto Kuriyagawa

Abstract Tool wear is one of the most critical problems in machining hard, brittle materials. In the present work, diamond turning experiments were performed on reaction-bonded silicon carbide, and the tool wear characteristics were investigated. A special kind of wear pattern, namely periodical groove wear, was identified on the flank face of the tool, where the periodicity of the microgrooves was the same as the tool feed. Geometrical analysis showed that the periodical groove wear was caused by the tool feed marks on the machined surface. Laser micro-Raman spectroscopy indicated that the high-pressure abrasive wear at the tool–workpiece interface dominates the wear behavior, rather than the diamond–graphite transformation. By swinging the tool around its curvature center during the cutting process, the periodical groove wear pattern was suppressed, and the tool wear was reduced significantly.

Keywords Silicon carbide · SiC · Hard, brittle material · Ductile machining · Diamond tool · Tool wear · Microgroove · Tool swinging · Laser Raman spectroscopy

1 Introduction

Silicon carbide (SiC) is an important material that has been extensively used in various harsh environmental conditions, such as high temperature, high pressure, and severe corrosion. Recently, in the optical manufacturing industry, reaction-bonded SiC (RB-SiC) is being used as mold material for high-precision hot pressing of glass lenses, for its high-temperature hardness, thermal shock resistance, and chemical stability [1]. On the other hand, RB-SiC has very poor machinability in ultraprecision machining. Conventionally, it has been machined by abrasive machining processes, such as grinding, lapping, and polishing [2–5]. Abrasive machining methods are capable of producing a fine surface finish, but it is very difficult to precisely fabricate microstructures [6] or complicated shapes which are increasingly demanded in industry. Other methods, such as laser ablation and focused ion beam milling, could be used to generate microstructures, but the material removal rate and finished surface quality cannot meet the requirements in optical applications [7, 8].

As an alternative approach, the ultraprecision diamond turning technology might be usable in fabricating microstructures and curved surface on RB-SiC. In a previous paper, we reported the material removal mechanisms in diamond turning of RB-SiC [9] and found that although RB-SiC is a typical hard, brittle material, it could be precisely machined in a ductile manner. Ductile machining of single-crystal SiC has been reported too [10]. However, diamond tools wore severely in the diamond turning process, which greatly degraded the finish surface quality as well as the form accuracy of the workpiece. Tool wear has become a major impediment to the industrial application of diamond turning of RB-SiC.

In this study, diamond turning tests on RB-SiC were performed, and fundamental tool wear characteristics were investigated. Tool wear patterns and their formation mechanisms were clarified, and possible techniques to suppress the tool wear and improve the service life of diamond tools were proposed.

Z. Zhang · J. Yan (✉) · T. Kuriyagawa
Department of Nanomechanics, Tohoku University,
Aramaki Aoba 6-6-01, Aoba-ku,
Sendai 980–8579, Japan
e-mail: yanjw@pm.mech.tohoku.ac.jp

Springer

2 Experimental details

2.1 Machine tool

Diamond turning experiments were carried out on a three-axis numerically controlled ultraprecision lathe, Nachi-ASP15, the main section of which is shown in Fig. 1. The machine tool has a hydrostatic bearing spindle and two perpendicular hydrostatic tables along the X-axis and the Z-axis. The B-axis rotary table is built into the X-axis table. After a renovation service of the numerical control system, the resolution of the X- and Z-axes was upgraded from 10 to 1 nm, and that of B-axis from 1/1,000° to 1/100,000°.

Before machining, the sample was bonded onto a copper blank using heat-softened wax, and then the blank was vacuum-chucked onto an air-bearing spindle. Thus, the sample was rotated with the spindle and moved along the Z-axis direction. A tool holder with a three-dimensionally adjustable mechanism was set on the rotary B-axis table. Diamond cutting tools were set onto the tool holder; thus, the tool can be moved along the X-axis direction and also rotated/swung around the B-axis. A CCD camera was equipped above the diamond tool to observe and adjust the position of the cutting point.

2.2 RB-SiC samples

RB-SiC samples used in the experiments were provided by Japan Fine Ceramics Co., Ltd. The samples were produced by infiltrating silicon melt into a green compact consisting of carbon powder and SiC particles with an average size of less than 1 μm. The liquid silicon reacts with carbon powders, forming new SiC particles. The infiltrated silicon does not react with carbon completely, and excessive silicon fills the remaining pores in the body so that a dense RB-SiC composite is produced [11]. The as-received samples were of cylindrical shape with polished end faces. The material properties of the samples are tabulated in Table 1. Figure 2 shows a scanning electron microscope (SEM) micrograph of the fast atom

Table 1 Material property of RB-SiC

| Property items	Value
Si/SiC volume ratio (%:%)	12:88
Density ρ (g/mm^3)	3.12
Young modulus E (GPa)	407
Bending strength R_T (MPa)	780
Thermal expansion coefficient (10^{-6}/K)	3.23
Thermal conductivity (W/m K)	143
Porosity	<0.1%

beam (FAB)-etched sample surface. The smooth regions correspond to SiC grains, and the micropits correspond to residual silicon. It can be seen that most of the SiC grains are directly bonded to each other without the presence of silicon at the grain boundaries.

2.3 Diamond cutting tools

Round-nosed cutting tools made of natural single-crystal diamond were used in experiments. Figure 3a presents the schematic diagram of the diamond tool. The tool has a nose radius of 10 mm, an edge length of 4 mm, a −20° rake angle ($\alpha=-20°$) and a 10° relief angle ($\gamma=10°$). As indicated in Fig. 3a, the crystallographic plane of the top surface of the tool is {110}, and the plane indicated by line MN, which is perpendicular to the top surface and passing the tool tip, is also {110}. Accordingly, the tool rake face is oriented close to the {210} plane. The tool flank face is curved; thus, its crystallographic plane changes with the position on the cutting edge. Two tools with the same shape and crystal orientation of the diamond, labeled as tool #1 and tool #2, respectively, were used. Before machining, the cutting edge was examined by SEM. Figure 3b shows an SEM micrograph of the fresh cutting edge, which is extremely sharp without visible defects even at a magnification of ×10,000.
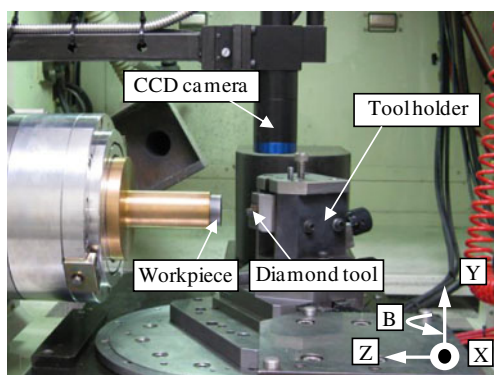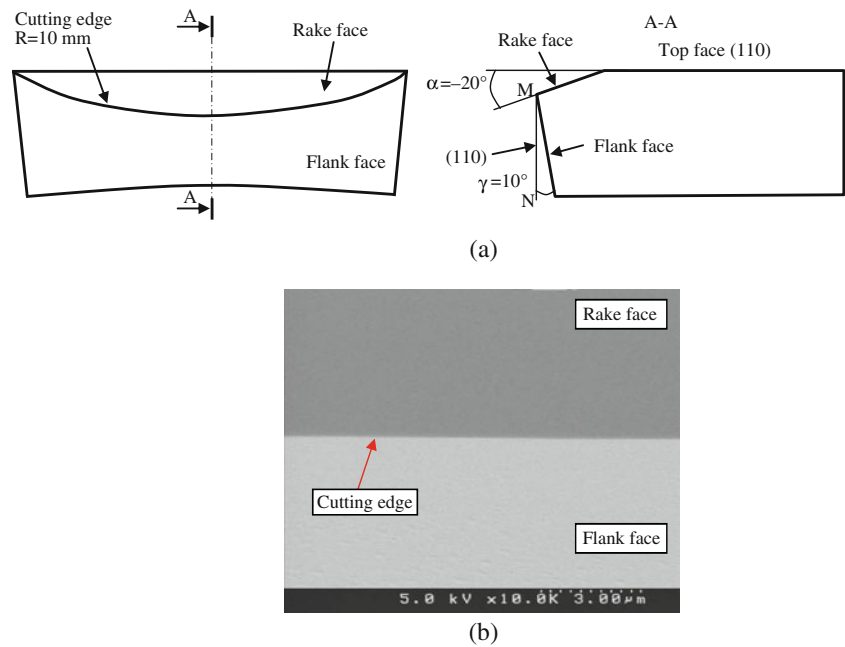

Fig. 1 Photograph of the experimental setup
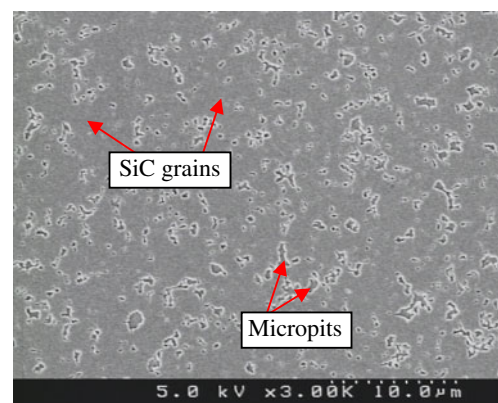
Fig. 2 SEM micrograph of an FAB surface-etched RB-SiC sample

Fig. 3 A round-nosed diamond cutting tool. **a** schematic diagram of the tool and **b** SEM micrograph of the cutting edge

(a)

(b)

It should be pointed out that natural diamond has the N, O, Co, Fe, and Ni elements inside its crystal, which leads to a different tool wear performance from that of a single-crystal diamond prepared by chemical vapor deposition. The diamond wear rate is also significantly different by crystallographic planes. The tools used in the present study have curved flank faces; thus, the crystallographic planes vary along the cutting edges, leading to different wear rates. The effects of chemical composition and crystallographic orientation of diamond on tool wear characteristics will be investigated in the future.
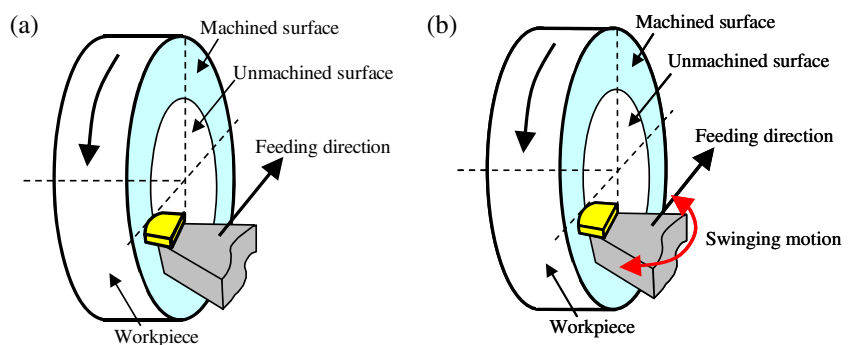
2.4 Cutting conditions

Face turning was carried out on the end faces of the samples. Two kinds of cutting tests were performed. One is the conventional cutting method without tool swinging, as shown in Fig. 4a. The other is the tool-swinging cutting method as shown in Fig. 4b. In the latter, the curvature center of the diamond tool is adjusted to agree with the center of the B-axis table, and the tool is swung around the B-axis center

during cutting. In this way, the cutting point is always changing along the cutting edge; thus, the temperature rise of the cutting edge can be reduced. The experimental conditions are listed in Table 2. The tools were examined after machining for a certain cutting distance (the total length of the cutting trace on the workpiece surface). Two levels of cutting distance (20 m and 136 m) were used to investigate the tool wear characteristics at the early stage and the late stage of a cut, respectively. In face turning, the cutting speed changes in a range of 94–19 m/min.

2.5 Surface characterization

In order to confirm if there are microstructural changes in the diamond tools after machining, the flank wear land of the tool was firstly examined using a laser micro-Raman spectroscope, NRS-3100, produced by JASCO Corporation (Tokyo, Japan). The wavelength of the laser was 532 nm, and the output laser power was set to 13 mW. The exposure time was set to 20 s, and the spot size of the laser beam was about 1 μm. After that,

Fig. 4 Schematic models for **a** conventional cutting method without tool swinging and **b** tool-swinging cutting method

(a)

(b)

Table 2 Experimental conditions

	No tool swinging		Tool swinging
	Tool #1	Tool #2	Tool #2
Feed rate f (μm/rev)	2	5	5
Maximum undeformed chip thickness t (nm)	40	100	100
Cutting distance l (m)	20	136	136
Tool-swinging speed ω (°/min)	0	0	25
Depth of cut d (μm)		2	
Spindle rotation rate (rpm)		1,000	
Cutting speed v (m/min)		94–19	
Cutting environment		Kerosene mist	

the diamond tools were Au–Pd coated for 30 s, and the flank wear land was examined using the SEM.

3 Experimental results

3.1 Tool wear pattern

Firstly, diamond tool #1 was used for machining with the left side of the tool contacting against the workpiece. After machining for a cutting distance of 20 m at f=2 μm/rev, a wear land as schematically shown in Fig. 5a was formed on the tool. Figure 5b shows an SEM micrograph of the wear land. The tool feed direction is from left to right in the figure. In Fig. 5b, we can see that the flank wear land is long and narrow, the maximum width of which is approximately 10 μm. At this magnification, the wear land surface looks uniform and nearly symmetrical about the tool tip. However, after a higher-magnification observation, it was found that the wear patterns on the left were distinctly different from those on the right. Figure 5c is a magnified view of the left side of the wear land. Extremely fine microgrooves, which are uniform in pitch and depth, can be observed on the wear land. This kind of wear pattern is defined as "periodical groove wear" in this paper. The orientation of the microgrooves is consistent with the cutting direction. It should be noted that due to the use of a negative rake angle, the rake face has been slanted; thus, the cutting direction is not perpendicular to the cutting edge, as shown in Fig. 5a. In Fig. 5c, it is also noticeable that the pitch of the microgrooves is 2 μm, the same as the tool feed per revolution of the workpiece. Besides the periodical groove wear, an extremely small crater wear (width ~1 μm) is also observed on the rake face. Fig. 5d shows a magnified SEM image of the right side of the flank wear land. Many scratched marks can be observed on the wear land, the orientation of which generally agrees with that of the microgrooves in Fig. 5c. However, the scratched marks in Fig. 5d do not show periodicity in pitch and

uniformity in depth, and the surfaces of the scratched marks are very rough. In contrast to the small crater wear in Fig. 5c, microchippings (size, ~2 μm) are observed on the rake face in Fig. 5d.

Next, diamond tool #2 was used for cutting. To compare with the results of tool #1, for tool #2, the tool feeding direction was from right to left. After cutting for a distance of 136 m at f=5 μm/rev, the tool was taken off for observation. Figure 6a shows schematically the location of the wear land. Figure 6b is an SEM micrograph of the flank wear land. The wear land is distinctly wider than that in Fig. 5b, and the shape of the wear land looks like a crescent. Figures 6c, d, and e are magnified views of three different locations as indicated in Fig. 6b. As shown in Fig. 6c, the left side of the wear land is very flat and smooth. This result is distinctly different from that in Fig. 5d, although both of the two sections contact with the shoulder region of the workpiece, namely the region between the machined surface and the unmachined surface. The reason of this difference will be discussed later in Section 4.

At the right side of the flank wear land, as shown in Fig. 6e, periodical microgrooves are observed. The grooves are uniform in pitch and depth, and the groove surfaces are very smooth. The orientation of the grooves is the same as the cutting direction, similar to that in Fig. 5c. However, different from Fig. 5c, the pitch between the grooves in Fig. 6e is 5 μm, equal to the tool feed per revolution of workpiece in this case. Figure 6d shows a boundary region between the smooth region and the grooved region.

3.2 Raman spectroscopy

The wear mechanism of a diamond tool is very complicated which might involve chemical, physical, electrical, and mechanical interactions between diamond and workpiece materials [12]. Also, diamond is known to undergo graphitization when it is subjected to high contact pressure (~100 GPa) in diamond–diamond indentation tests [13].

Fig. 5 Tool wear after a cutting distance of 20 m at $f=2$ μm/rev. **a** schematic diagram showing the location of the wear land. **b** SEM micrograph of the entire flank wear land. **c** and **d** are close-up views of the left side and the right side of the wear land, respectively
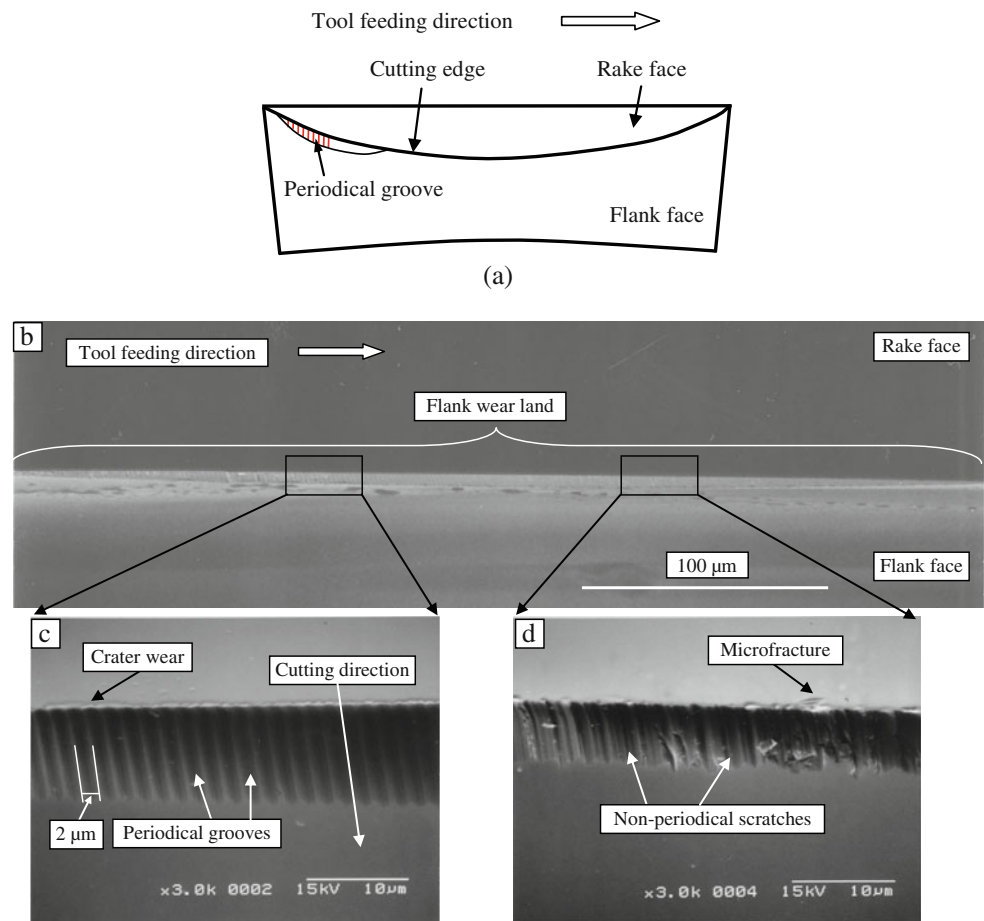
According to the material hardness comparison, the pressure at the tip of the diamond tool in RB-SiC cutting should be lower than the diamond–diamond contact pressure (~100 GPa) but higher than the pressure in silicon cutting (~10 GPa) [14]. In this work, to investigate possible microstructural changes of the diamond, we examined the wear land using laser micro-Raman spectroscopy.

Figure 7 shows a Raman spectrum of the wear land (the lower curve, corresponding to the left-side intensity scale) and a replot of the same spectrum at a magnified intensity scale (the upper curve, corresponding to the right-side intensity scale). There is a strong sharp peak at 1,332 cm^{-1} that corresponds to the first-order Raman peak of crystalline diamond (1,332.4 cm^{-1}) [15]. Residual stress might exist inside the diamond tool, but it could not be detected using the present Raman spectroscope system which has a Raman shift resolution of 1 cm^{-1}. It has been known that in crystalline graphite, a sharp peak at 1,580 cm^{-1} (G band) is observed, and in microcrystalline graphite, this is accompanied by a band at around 1,350 cm^{-1} (D band) [16]. In Fig. 7, however, no peaks could be observed at 1,580 cm^{-1} and 1,350 cm^{-1}. Therefore, under the present experimental conditions, there is no direct evidence showing that the

diamond–graphite transformation takes place on the flank wear land when cutting RB-SiC. Although a broad band at 1,450 cm^{-1} is observed in Fig. 7, which indicates the presence of non-diamond carbon [16], it is hard to say that this non-diamond carbon is caused by machining. The same broad band could be found on the surface of an unused diamond tool.

4 Discussion on groove wear mechanism

The experimental results in Section 3 have demonstrated that microgroove wear is a dominant wear pattern in diamond turning of RB-SiC. Such groove wear has also been reported in diamond turning of other hard materials such as single crystalline silicon [17–19]. There are a number of hypotheses on the formation mechanism of groove wear. For example, through molecular dynamics simulation, Cai et al [18] found that a kind of "dynamic hard particles," which were formed by the silicon atom groups with much shorter bond lengths, plough on the softened flank face of the diamond tool and lead to the groove wear. Zong et al. [19] reported that two kinds of hard particles, namely, SiC and diamond-like carbon, were
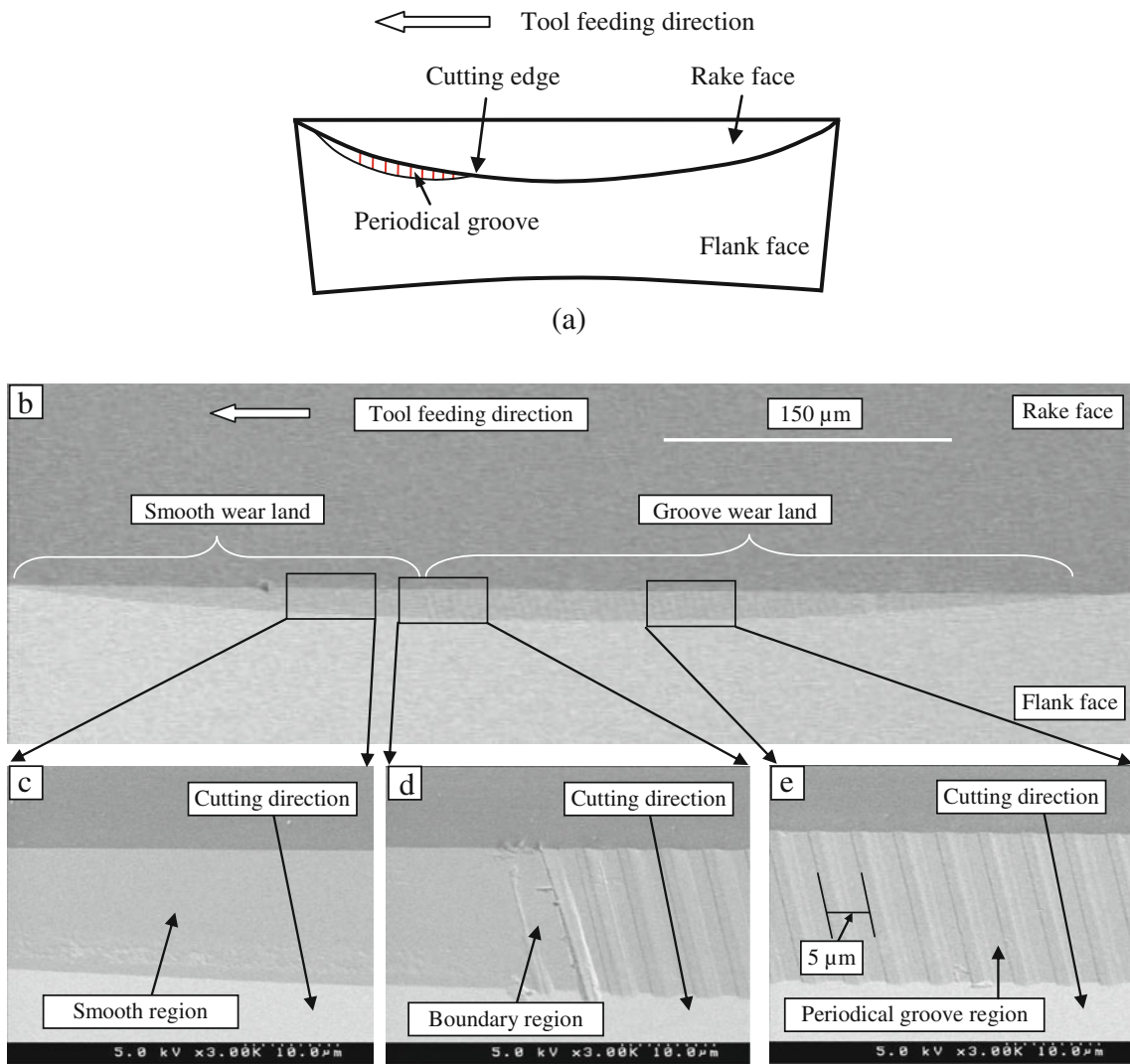
Fig. 6 Tool wear after a cutting distance of 136 m at f=5 μm/rev. **a** schematic diagram showing the location of the wear land. **b** SEM micrograph of the entire flank wear land. **c**, **d**, and **e** are close-up views of different locations of the wear land
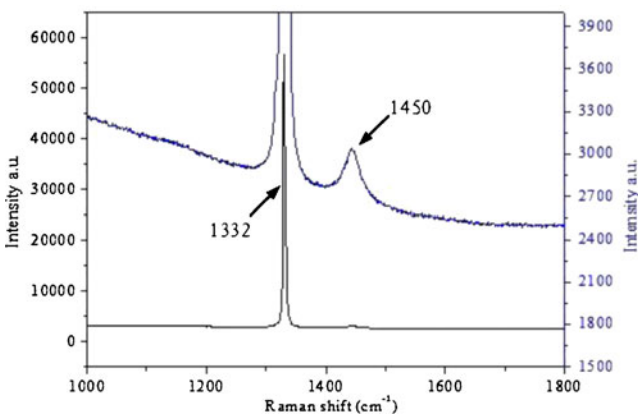
Fig. 7 Raman spectrum of a wear land on the diamond tool. The upper curve is a replot of the lower curve with a magnified intensity scale

generated during diamond turning of silicon. Those particles scratch and plough on the tool flank face so as to form the groove marks. These hypotheses could give a satisfactory explanation of the randomly distributed groove wear in silicon machining, but could not explain the generation of periodical groove wear.

In this study, from the fact that the pitch of the microgrooves is the same as the tool feed, we presume that the groove wear is a result of replication from the tool feed marks on the machined surface. Figure 8 shows a schematic model for diamond turning using a new round-nosed tool, and Fig. 9 shows schematically the material removal and deformation model. When a new tool is used, only the right-hand part of the cutting edge contacts with the workpiece. As undeformed chip thickness varies along the cutting edge from zero to a maximum value from the left to the right, there will be four regions under different material
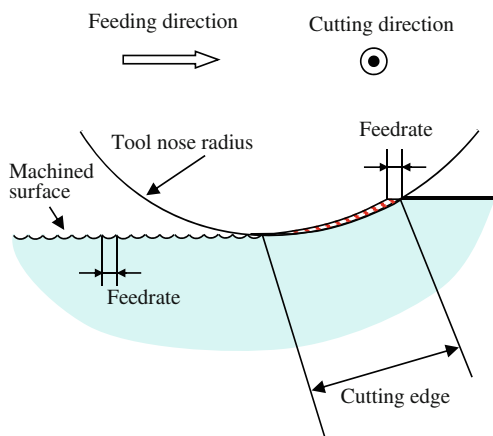
Fig. 8 Schematic model for diamond turning using a new cutting tool

Fig. 10 Schematic model for the generation mechanism of periodical grooves on flank wear land

deformation mechanisms, namely rubbing, plastic deformation, plowing, and cutting. Material removal only occurs in the "cutting" region. In other regions, no material is removed, and only squeezing between the tool and the workpiece takes place. As a result, a high-pressure and high-temperature condition will be generated at the tool–workpiece interface, which leads to severe friction between the tool and the workpiece.

The hardness of diamond is 10,000 HV, and that of SiC is 3,000 HV. Thus, when the two materials are in contact and undergo friction, the wear rate of diamond should be lower than that of SiC. In a diamond turning process, however, the area of the diamond tool tip is far smaller than the workpiece area. That is, a small-area tool tip is continuously rubbed and scratched by a large-area SiC disc. This situation will finally wear away a significant volume of diamond, leading to edge retreat and scratch marks on the wear land of the diamond tool.

After the tool tip retreat has begun, the flank wear land will extend gradually towards the left side of the tool, as shown in Fig. 10. Finally, the originally round-nosed tool would be worn into a partially straight one. Accordingly, as the cutting tool is fed from the left to the right in Fig. 10, the machined surface with periodical tool feed marks will
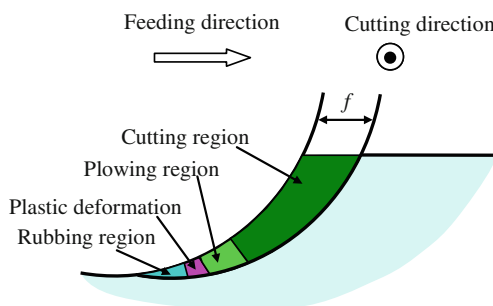

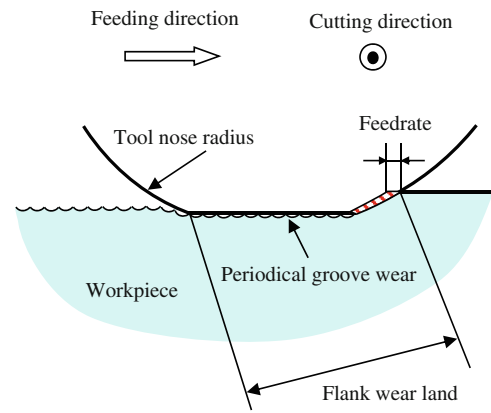**Fig. 9** Schematic model for material removal/deformation in the cutting region

continuously squeeze the flat wear land, and the periodical tool feed marks on the machined surface will be replicated onto the flank wear land of the tool, leaving micro-periodical grooves.

It should be noted that periodical groove wear only occurs to the flat region of the cutting edge on the left hand in Fig. 10. The right-hand side of the tool contacting with the shoulder region of the workpiece will be randomly scratched by the SiC grains, leading to a non-periodical scratching wear pattern as shown in Fig. 5d. In addition, as the cutting distance increases further and the tool tip retreat reaches the similar level to the nominal depth of cut, the effective depth of cut approaches zero. In this case, no material will be removed, and the tool wear land will only rub over the unmachined surface, which can flatten and smoothen the wear land, as shown in Fig. 6c. From this opinion, the tool wear in diamond turning of RB-SiC, also of other ultra-hard materials, must be considered as a dynamically changing process.

5 Tool-swinging cutting tests

Finally, the tool-swinging cutting method shown in Fig. 4b was adopted in the present work. The diamond tool #2 was used for cutting at $f=5$ μm/rev, and its tool wear characteristics were compared with those of the conventional method. Figure 11a shows an SEM micrograph of the flank wear land after a cutting distance of 136 m, and Figs. 11b, c, and d are magnified views of three different regions of the wear land. It can be seen that the width of the flank wear land is almost uniform and is distinctly smaller than that in Fig. 6b. The scratch marks on the wear land show no periodicity.

Table 3 shows a comparison of tool wear rates in terms of flank wear width, tool edge retreat, and tool wear volume between the conventional cutting method and the tool-
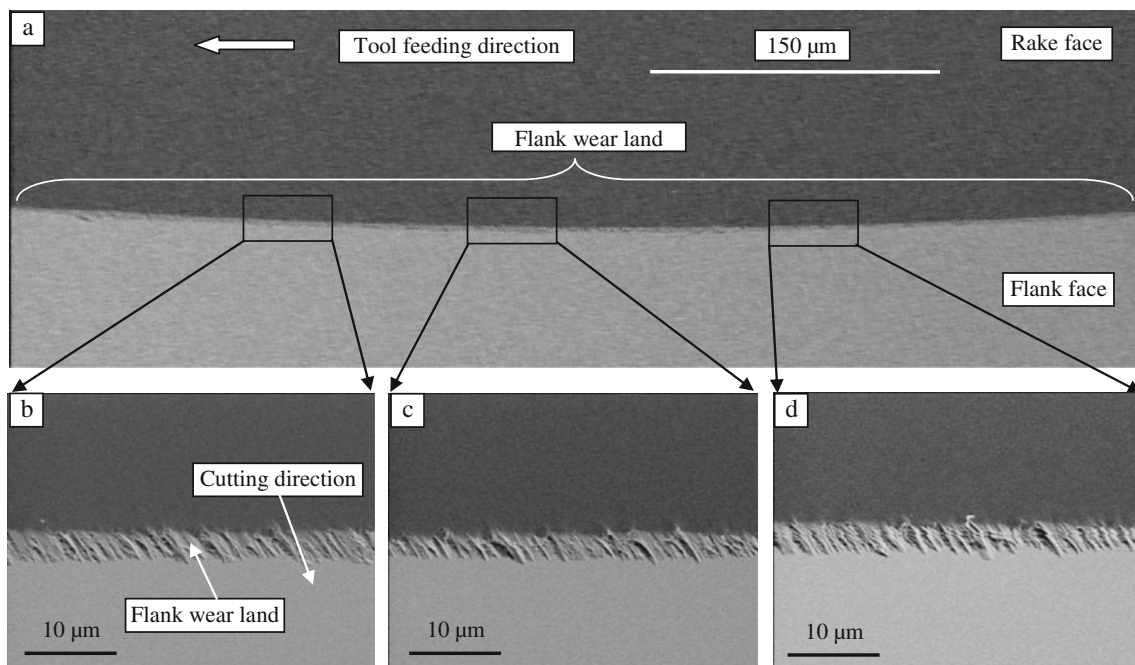
Fig. 11 SEM micrographs of the cutting edge after a cutting distance of 136 m by the tool-swinging cutting method. **a** general view of the flank wear land. **b**, **c**, and **d** are close-up views of three different regions of the flank wear land

swinging cutting method. Flank wear width was directly measured from the SEM micrographs. Tool edge retreat was calculated from the relief angle and the measured flank wear width. Tool wear volume was calculated using the 3-D CAD software CATIA V5 (Dassault Systèmes, S.A., France) based on the tool wear geometry measured from the SEM micrographs of the tool. Due to tool swinging, the flank wear width and the tool edge retreat have been reduced from 15.8 to 2.8 μm and from 2.8 to 0.5 μm, respectively. The tool wear volume in the tool-swinging method is 2,417 μm³, about 40% of that in the conventional cutting method. Therefore, the tool wear has been not only distributed, but also totally reduced. As a result of tool swinging, the machined surface roughness has been improved from 46 nm Ra to 9 nm Ra. The significant decrease in the retreat of tool edge in the tool-swinging cutting method will facilitate the improvement of work-piece form accuracy that was deteriorated by severe tool wear in the conventional cutting method.

The tool-swinging motion provides a continuous change of cutting point along the cutting edge; thus, the cutting time for a certain cutting point becomes very short. In addition, the cutting edge can be effectively cooled during the air-cut period so that the temperature rise of the cutting edge will be significantly reduced. In addition, the tool can be well lubricated as it swings, because lubricants can easily penetrate into the tool–workpiece interface. There-fore, the tool-swinging cutting method might be an effective method to reduce tool wear in diamond turning of ultra-hard materials, although the tool-swinging motion makes the operation sophisticated. The workpiece form error induced by the tool-swinging error can be eliminated by numerical control program compensation. Further investigation of the tool-swinging cutting method will be reported in another paper elsewhere.

6 Conclusions

Tool wear characteristics in diamond turning of RB-SiC have been studied by SEM observation and micro-laser Raman analysis. The following conclusions have been drawn:

1. Flank wear is significant. The flank wear land consists of two regions having different wear patterns: periodical microgrooves and non-periodical scratch marks. The non-periodical scratch marks may disappear as the cutting distance increases.

Table 3 Comparison of tool wear rates between conventional cutting and tool-swinging cutting

	No tool swinging	Tool swinging
Flank wear width (μm)	15.8	2.8
Tool edge retreat (μm)	2.8	0.5
Tool wear volume (μm³)	5,994	2,417
Surface roughness Ra (nm)	46	9

2. The microgrooves on the wear land are oriented along the cutting direction, and the pitch of the grooves is the same as the tool feed per revolution of the workpiece. The grooves are replicated from the tool feed marks on the machined surface.

3. Raman spectroscopy of the wear land shows that the diamond–graphite transformation does not occur during machining. The dominant wear mechanism is the abrasive scratching effect of the SiC grains at the tool–workpiece interface.

4. The tool-swinging cutting method can significantly reduce tool wear and remarkably improve the cutting performance of the tools.

References

1. Hall C, Tricard M, Murakoshi H, Yamamoto Y, Kuriyama K, Yoko H (2005) New mold manufacturing techniques. Proc SPIE 5868:58680V

2. Toshiya H, Ichiro I, Junichi S (1985) Grinding of silicon carbide with diamond wheel, T. Jpn Soc Mech Eng C 51:1864–1870

3. Dai Y, Ohmori H, Lin W, Eto H, Ebizuka N, Tsuno K (2005) ELID grinding properties of high-strength reaction-sintered SiC. Key Eng Mater 291–292:121–126

4. Tam HY, Cheng HB, Wang YW (2007) Removal rate and surface roughness in the lapping and polishing of RB-SiC optical components. J Mater Process Tech 192–193:276–280

5. Cheng H, Feng Z, Lei S, Wang Y (2005) Magnetorheological finishing of SiC aspheric mirrors. Mater Manuf Process 20:917–931

6. Yan J, Oowada T, Zhou T, Kuriyagawa T (2009) Precision machining of microstructures on electroless-plated NiP surface for molding glass components. J Mater Process Tech 209:4802–4808

7. Samant A, Dahotre N (2009) Laser machining of structural ceramics. J Eur Ceram Soc 29:969–993

8. Wesch W, Heft A, Menzel R, Bachmann T, Peiter G, Hobert H, Höche T, Dannberg P, Bräuer A (1999) Ion beam processing of SiC for optical application. Nucl Instrum Meth B 148:545–550

9. Yan J, Zhang Z, Kuriyagawa T (2009) Mechanism for material removal in diamond turning of reaction-bonded silicon carbide. Int J Mach Tools Manuf 49:366–374

10. Patten JA, Gao W, Yasuto K (2005) Ductile regime nanomachining of single-crystal silicon carbide. J Manuf Sci E-T ASME 127:522–532

11. Suyama S, Kameda T, Itoh Y (2003) Development of high-strength reaction-sintered silicon carbide. Diam Relat Mater 12:1201–1204

12. Ohta T, Yan J, Kodera S, Yajima S, Horikawa N, Takahashi Y, Kuriyagawa T (2008) Coolant effects on tool wear in machining single-crystal silicon with diamond tools. Key Eng Mater 389–390:144–150

13. Gogotsi G, Kailer A, Nickel G (1999) Transformation of diamond to graphite. Nature 401:663–664

14. Yan J, Asami T, Harada H, Kuriyagawa T (2009) Fundamental investigation of subsurface damage in single crystalline silicon caused by diamond machining. Prec Eng 33(4):378–386

15. Vogelgesang R, Alvarenga AD, Kim H, Ramdas AK, Rodriguez S, Grimsditch M, Anthony TR (1998) Multiphonon Raman and infrared spectra of isotopically controlled diamond. Phys Rev B 58:5408–5416

16. Nazare MH, Neves AJ (2001) Properties, Growth and Applications of Diamond. INSPEC, IEE, London

17. Yan J, Syoji K, Tamaki J (2003) Some observations on the wear of diamond tools in ultraprecision cutting of single-crystal silicon. Wear 255(7–12):1380–1387

18. Cai MB, Li XP, Rahman M (2007) Characteristics of "dynamic hard particles" in nanoscale ductile mode cutting of monocrystalline silicon with diamond tools in relation to tool groove wear. Wear 263:1459–1466

19. Zong WJ, Sun T, Li D, Cheng K, Liang YC (2008) XPS analysis of the groove wearing marks on flank face of diamond tool in nanometric cutting of silicon wafer. Int J Mach Tools Manuf 48:1678–1687